Sammalkorpi, Maria; Sanders, Samantha; Panagiotopoulos, Athanassios; Karttunen, Mikko; Haataja, Mikko

Simulations of micellization of sodium hexyl sulfate

Published in:
Journal of Physical Chemistry B

DOI:
10.1021/jp109882r

Published: 01/01/2011

Document Version
Early version, also known as pre-print

Please cite the original version:
Sammalkorpi, M., Sanders, S., Panagiotopoulos, A., Karttunen, M., & Haataja, M. (2011). Simulations of micellization of sodium hexyl sulfate. Journal of Physical Chemistry B, 115(6), 1403-1410. https://doi.org/10.1021/jp109882r

J. Phys. Chem. B, 2011, 115 (6), pp 1403–1410
DOI: 10.1021/jp109882r
http://pubs.acs.org/doi/abs/10.1021/jp109882r

Simulations of micellization of sodium hexyl sulfate

M. Sammalkorpi[1,*], S. Sanders[2], A. Z. Panagiotopoulos[2], M. Karttunen[3], and M. Haataja[4]

[1] Department of Chemical and Environmental Engineering, Yale University, New Haven, USA and Department of Chemistry, Aalto University School of Science and Technology, Finland
[2] Department of Chemical and Biological Engineering, Princeton University, Princeton, USA
[3] Department of Applied Mathematics, The University of Western Ontario, London, Ontario, Canada
[4] Department of Mechanical and Aerospace Engineering, Princeton University, Princeton, USA

[*] Formerly M. Huhtala

Abstract

Micellization of the ionic surfactant sodium hexyl sulfate has been studied using atomistic explicit-solvent molecular dynamics simulations with and without excess NaCl or $CaCl_2$. Simulations were performed at surfactant loadings near the critical micellization concentration. Equilibrium micelle size distributions and estimates of the critical micellization concentration obtained from the simulations are in agreement with experimental data. In comparison to the sodium dodecyl sulfate surfactant, the shorter alkyl chain of sodium hexyl sulfate results in increased disorder of the micellar core and water exposure of the hydrocarbon tail groups.

However, water and ions do not penetrate into the micellar core even for these weakly micellizing surfactants. Excess NaCl is observed to have a minor influence on the micelle structure but excess $CaCl_2$ induces drastic changes both in the structure and the dynamics of the micellar system. Furthermore, in the absence of excess salt, sodium hexyl sulfate forms predominantly spherical, disorganized aggregates but an increase in ionic strength drives an increase in aggregate size and leads to prolate aggregates.

1 Introduction

Micellization is a self-assembly phenomenon that is common to solutions of amphiphilic molecules (surfactants), proteins, peptides, and block copolymers above a certain concentration[1]. Depending on temperature, surfactants form insoluble crystals or micelles[2,3] and may also aggregate to more complex phases, such as cubic or lamellar[1,3–7]. Surfactants are used in detergency, oil purification processes, nanotechnology applications such as nanocarriers in drug-delivery[8,9], emulsions and foams[10], and even in nanolithography[1].

The general mechanism of micelle formation as an interplay between solvophobic and solvophilic interactions is well understood. However, control and manipulation of the microscopic details of micelle structure in solution and the micellization process are still of interest for applications. Simulations provide an accessible means of obtaining such information. Micellization has been studied mostly by lattice and off-lattice coarse-grained models[11–22]. More recently, atomistic studies with and without solvent have emerged[23–34].

Two significant issues are encountered in simulations of micellization. For most common surfactants, micelle formation timescales are microseconds or longer and critical micellization concentrations are of the order $1-100$ mMol. Consequently, coarse-grained models (typically in implicit solvent) are often employed in order to achieve equilibration at concentrations close to the critical micellization concentration (CMC). For example, Lazaridis et al. have studied DPC micelle formation[34] and Jusufi et al. sodium alkyl sulfate micellization[20,21] in an implicit solvent environment. For molecular level coarse-grained and atomistic systems with explicit solvent, our previous work of Ref.[22] has yielded micellization results on microsecond time scale on multimicellar

coarse grained systems, and most related to this work, Refs.[31,33] on atomistic multimicellar systems. Micelles in the latter simulations emerged from a random initial positioning of sodium dodecyl sulfate (SDS) molecules in aqueous solution at 200 mMol, 700 mMol, and 1 Mol concentrations with varying salt concentrations. However, the experimental CMC for SDS is much smaller, 8 mMol$\pm$1.4 mMol, depending on measurement[35–40], and the 200 ns duration of the simulations of Refs.[31,33] is insufficient to fully equilibrate the SDS system.

In the present study, we overcome time scale and concentration issues by choosing a surfactant, sodium hexyl sulfate (SHS), for which the CMC at 25 degrees Celsius has been reported as 420 mMol[41] or 517 mMol[42] and the rate constants describing micellar reorganization dynamics are of the order $10^9 s^{-1}$ [3]. These values are such that although they are challenging for current atomistic molecular dynamics simulations, they can be achieved with some effort, as will be demonstrated below. More specifically, we study SHS micellization and micelle structure at conditions close to the critical micellization concentration with simulation durations sufficient to equilibrate the distribution. In the case of ionic surfactants, the concentration and type of excess salt provides another means to control the aggregate structure and properties. Here, we probe the effects of NaCl and $CaCl_2$ on micellar structure, size distribution, and equilibration processes. We also compare the results with those for longer chain sodium alkyl sulfates, even though the longer surfactant simulations are well above their corresponding CMCs and have not reached equilibrium. To our knowledge, these are the first atomistic simulations of surfactant systems with explicit solvent and ions that achieve timescales required for system equilibration at concentrations comparable to experimentally reported CMCs.

1.1 Computational Model

The Gromacs 3.3 simulation package[43–45] with the united atom parametrization was employed for the atomistic molecular dynamics (MD) simulations. The energies of the initial configurations were minimized with the steepest descent method. After the initialization, all simulations were performed in the NpT ensemble at $p = 1$ bar using the weak coupling method for pressure and temperature control[46]. The coupling times were set to 1.0 ps for pressure and 0.1 ps for temperature, and the temperatures of

the solute, counterions, and solvent were controlled independently. The bond lengths of the surfactant molecules were constrained by the LINCS algorithm[47] and those of the water molecules by SETTLE[48]. A time step of 2 fs was used in all simulations reported here. The Lennard-Jones interactions were cut off at 1 nm with no extended long-range modifications and the full particle-mesh Ewald method[49] was employed for the long-ranged electrostatic interactions; not fully accounting for these long-ranged electrostatic interactions has been shown to lead to serious artifacts in the simulations of amphiphilic molecules[50,51] and contrary to the rather common misconception, proper treatment of electrostatics is also computationally efficient[52].

The SHS parametrization is not part of the standard Gromacs force-field. Since SHS and SDS differ only by number of methyl groups in the hydrocarbon tail (6 vs. 12), we adopt the SDS parametrization discussed and validated in detail in Ref.[31] for SDS with the only difference here being the shorter hydrocarbon tail length. The sodium, calcium, and chloride ions were described by the Gromacs parameters; for a detailed discussion of ionic parameters, please see Refs.[53,54]. The Simple Point Charge (SPC) water model[55], which is consistent with the chosen force field, was adopted for the water molecules. Visualizations of all molecular configurations were generated with VMD (Visual Molecular Dynamics)[56].

Since the micelle-forming systems studied here typically have multiple micelles, and micelle properties are computed for a given micelle, the data analysis relies on identifying to which micelle each SHS molecule belongs. The micelle classification scheme is based on a geometrical distance criterion: any two surfactants with methyl groups closer than $R_{cut} = 0.4$ nm are classified as belonging to the same micelle. The weakly micellizing SHS is sensitive to the choice of this cut-off distance. This geometric criterion is different from that used in our prior SDS micellization studies[31–33] because it provided better agreement with visual observations and consistent estimates of the critical micellization concentration, see Section 2. The statistical uncertainties of the critical micellization concentration are derived from the standard deviation of the block averages where the data sample was divided into 5 blocks. The statistical uncertainties of the radii of gyration and the moments of gyration have been estimated from the standard deviation of the data sample.

1.2 Simulated system

We have studied systems containing 200 SHS molecules at a random initial configuration solvated to 700 mMol concentration or 1 Mol concentration in the presence of two different levels of excess salt (NaCl and $CaCl_2$). SHS consists of an Na^+ ion released in aqueous solution and the anionic hexylsulfate molecule, see Fig. 1. Thus, even in the absence of excess salt, a solution of SHS contains free Na^+ counterions. The systems studied contained either no excess salt (i.e., only Na^+ ions were present to neutralise the sulfate head groups), 50 excess NaCl or $CaCl_2$ molecules, or 200 excess NaCl or $CaCl_2$ molecules. In terms of ionic concentrations, these systems correspond to $175/700$ mMol (for the 700 mMol SHS systems) or 250 mMol/1 Mol (for the 1 Mol SHS systems). To evaluate the effects of the system size, simulations of 400 SHS molecules at 700 mMol and 1 Mol concentrations with no excess salt were also performed. The number of water molecules ranged between 8170 and 14448.

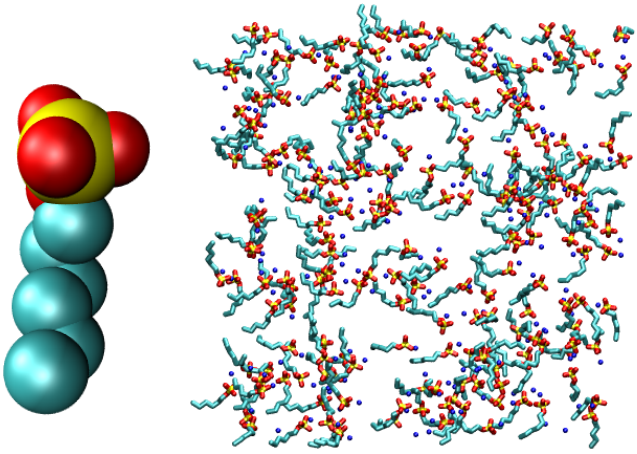

Figure 1: Left: The hexylsulfate molecule. Right: An example of the random initial configuration, a 700 mMol 200 SHS system without excess salt. The 14448 water molecules have been omitted in the visualization.

Initially, the SHS molecules are placed randomly in the simulation box with the sodium counterions close to the SHS head groups, see Fig. 1. Next, the simulation box was filled with water. In the simulations with excess salt, the ions were introduced by replacing randomly chosen water molecules. Subsequently, the total energy was mini-

mized using the steepest descent algorithm. Temperature was maintained at 323 K. To evaluate the potential influence of the initial configuration on the resulting micelle distribution, comparison simulations at 700 mMol and 1 Mol SHS concentrations starting from a micellized initial configuration were also studied. The initial configurations of micelles were obtained from the final configurations of the simulation of the initially random 200 SHS systems with 200 $CaCl_2$ molecules. The excess $CaCl_2$ was removed from these configurations and the holes were filled with water. These initially larger micelles were left to evolve an additional 200 ns, after which the resulting distribution was compared with the corresponding 700 mMol and 1 Mol systems with 400 and 200 SHS molecules in which the simulation run had been started from an initially random configuration.

We also compared the SHS results with the micellization behavior of the longer chain sodium dodecyl sulfate (SDS). The SDS simulations used as comparison data contain 400 SDS molecules in 700 mMol solution with either no excess salt or excess 700 Mol NaCl or $CaCl_2$ simulated for 200 ns. The details of the SDS simulations are discussed in Ref.[33].

2 Results

2.1 SHS micellization and micelle size distribution

The left panel of Figure 2 shows the configuration of the micellized 200 SHS system at 1 Mol concentration after 200 ns of simulation. The right panel shows the micelle size distribution obtained as time average over the period from 40 ns to 200 ns of simulation time. System sizes of 200 and 400 SHS molecules at approximately 1 Mol concentration starting either from a random initial configuration or an initial configuration in which the SHS are already aggregated to micelles are shown. The distributions with different systems sizes and initial configurations at 700 mMol SHS concentration are practically superimposed with the peak shifted toward smaller aggregates. This forms an extension to the oligomer peak. The figure shows that micellization takes place resulting in an aggregate distribution in which a significant portion of the molecules are present as oligomers. As the aggregate size increases there is a local minimum in the distribution followed by another peak, which corresponds to the micellization

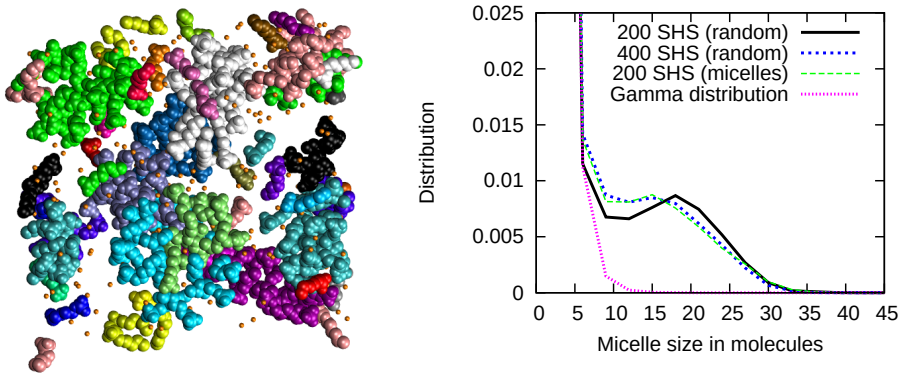

Figure 2: The left panel shows the configuration of the micellized 200 SHS system at 1 Mol concentration after 200 ns of simulation. The different colors indicate micelle classification, i.e., SHS molecules are colored according to the micelle they are in. The right panel shows the micelle size distribution obtained as time average over the period from 40 ns to 200 ns of simulation time in systems of 200 and 400 SHS molecules at approximately 1 Mol concentration starting either from a random initial configuration or an initial configuration in which the SHS are already aggregated to micelles. The Gamma distribution shown is used to approximate the number of nonaggregated surfactants in the system. The distribution presented here is fitted to the data set of 200 initially randomly distributed SHS molecules.

peak. The distribution graphs show that the resulting distributions are independent of the initial starting configuration (random vs. initially micellized). The variation in the curve peak position actually originates from a difference in concentration, i.e., due to technical limitations in setting up the simulations at *exactly* 1 Mol concentration. The concentrations calculated at 200 ns in the three simulations are 0.96 Mol, 0.97 Mol, and 1.03 Mol with the nearly superimposed curves corresponding to the two smaller concentrations and 400 SHS and initially micellized 200 SHS molecules. The systems of different size and different initial configuration provide nearly superimposed distributions following the concentration. Thus we conclude that using the smaller system containing 200 SHS molecules for the simulations is sufficient to probe the equilibrium micelle distribution. We choose to use the random initial configuration even though the comparison shows that the simulation duration is sufficient to produce a micelle size distribution that is independent of the initial configuration (random vs. micellized).

In earlier work[31], we have validated the simulation model for SDS, which differs from SHS only in hydrocarbon chain length. Due to time scale limitations with respect to SDS relaxation, we were not able to obtain the critical micellization concentration (CMC) for SDS. The CMC is highly sensitive to chain length. For SHS, which has faster timescales in its dynamics, we are able to obtain the CMC; results are presented in Table 1. Calculated CMC values for the systems without excess salt are close to the experimentally measured CMC values of 420 mMol[41] and 517 mMol[42]. However, there is a decrease in the CMC from 360 ± 30 mMol to 300 ± 10 mMol when going up in overall SHS concentration from 700 mMol to 1 Mol. Notably, CMC depends on how one measures it; this is seen both in experiments and simulations. In our case, we define the CMC from the total concentration of oligomers present at equilibrium with the aggregates[62]. In Ref.[62], it has been shown using simulations that the concentrations of oligomers correspond closely to the CMC values obtained from the osmotic pressure curve. The underlying implication is that the volume fraction of free surfactant is constant or increases slightly with concentrations at or above CMC. The oligomer concentration can change when the overall concentration of surfactant changes. The observed decrease is partly due to there being less "free volume" for monomers and oligomers at higher concentrations and partly to solution nonidealities. The CMC decreases with increased ionic strength. This is a characteristic of ionic surfactants, see for example Refs.[57–61]. Although the 700 mMol and 1 Mol SHS systems with excess

salt are not at the same ionic strength, and thus the values cannot be compared directly, the decreasing trend in the CMC with increasing ionic strength is evident.

The CMC estimates presented here have been calculated using the idea that the concentration of nonaggregated surfactants, predominantly monomers and dimers, can be used as an approximation of the CMC[62]. We obtained the oligomer concentrations from the aggregate size distribution data presented for 1 Mol systems in Fig. 3. The curves are normalized so that the distribution value multiplied by the aggregation number over the entire curve is equal to 1. The 700 mMol systems are analogous, although in low ionic strength, the distribution curves do not have a distinct aggregation peak. We can still observe that an aggregation peak exists indicating micellization does occur at this concentration, but it is significantly overlapping with the nonaggregated peak and therefore we can not simply choose a cutoff aggregation value for determining which oligomers are considered aggregated and which are considered nonaggregated. Due to this fact, we chose to approximate the nonaggregated part of the curve by a distribution. The Gamma distribution ($C_\Gamma \frac{1}{\beta^\alpha \Gamma(\alpha)} x^{\alpha-1} e^{(-x/\beta)}$) was chosen as the best fit in comparison to a Poisson distribution ($C_P \lambda^x e^{-\lambda}/x!$) or exponential distribution ($C_E \lambda e^{-\lambda x}$) by using the squared difference between the calculated distribution values and the actual aggregate size distribution values from the simulation as the measure of the goodness of fit. In all distribution equations above, C is a constant to scale the probability distribution, x is the distribution variable, and α, β, and λ are parameters to be fitted. The parameters for the distributions were determined by matching the values of the distributions to the first two points of the aggregate size distribution, which due to grouping, represented all aggregates of six surfactants or less. Although, in many cases, the Gamma distribution was negligibly different from the exponential distribution, the Gamma distribution has one more parameter than the exponential distribution. This can, at times, help achieve a better fit and may even be useful for matching more than two points.

After the parameters were determined, the entire Gamma distribution was used to determine the number of surfactants considered to be nonaggregated by taking each value of the distribution and multiplying it by both the corresponding aggregate size and the total number of surfactants. The number of nonaggregated surfactants was divided by the volume of the system to determine the concentration. The concentration of the nonaggregated surfactants is the approximation of the CMC. For the CMC estima-

tion, we analyzed simulation trajectories using different micelle classification cut-off values R_{cut} and concluded that the estimates are sensitive to the choice of R_{cut} in this weakly micellizing system. Consistent estimates of critical micellization concentration values were obtained by using a cut-off value of $R_{cut} = 0.4$ nm, where a larger R_{cut} value of 0.45 nm produces large apparent variations in the CMC between different simulated systems. Smaller R_{cut} values (e.g. 0.35 nm) were also tried, but resulted in classification which no longer agreed with visual analysis. This cut-off sensitivity appears because the CMC is calculated from the monomer and oligomer concentrations which are sensitive to the classification cut-off because the aggregates micellize weakly; SHS molecules are loosely bound to micelles. There is much less sensitivity for the larger aggregate sizes, the micellization peak position, and correspondingly, micelle structural properties calculated from the larger aggregates. The more strongly micellizing SDS, which has significantly fewer monomers and oligomers in a micellized solution, see for example[31,33], does not exhibit such sensitivity. Although we choose to use $R_{cut} = 0.4$ nm in the classification, as it causes less discrepancy between the CMC values of the 700 mMol and 1 Mol systems, we note that the choice is somewhat arbitrary and the micellization distribution is sensitive to the choice. Experimental measurements in such a weakly micellizing system could also suffer from similar sensitivity, for example, to small changes in solution conditions such as impurities in experimental measurements.

Table 1: Critical micellization concentrations (CMC) using $R_{cut} = 0.4$ nm.

System	700 mMol SHS CMC in Mol	1 Mol SHS CMC in Mol
no excess salt	0.36 ± 0.03	0.30 ± 0.01
50 NaCl ($175/250$ mMol)	0.32 ± 0.01	0.26 ± 0.01
200 NaCl (700 mMol $/1$ Mol)	0.24 ± 0.01	0.18 ± 0.01
50 $CaCl_2$ ($175/250$ mMol)	0.22 ± 0.01	0.21 ± 0.02
200 $CaCl_2$ (700 mMol $/1$ Mol)	0.10 ± 0.01	0.09 ± 0.01

The ionic strength of the solution has a large influence on the micellization and micelle size distribution formed in the simulation. A visual analysis of the final (200 ns) simulations configurations shows that the micelles formed in the presence of $CaCl_2$ are

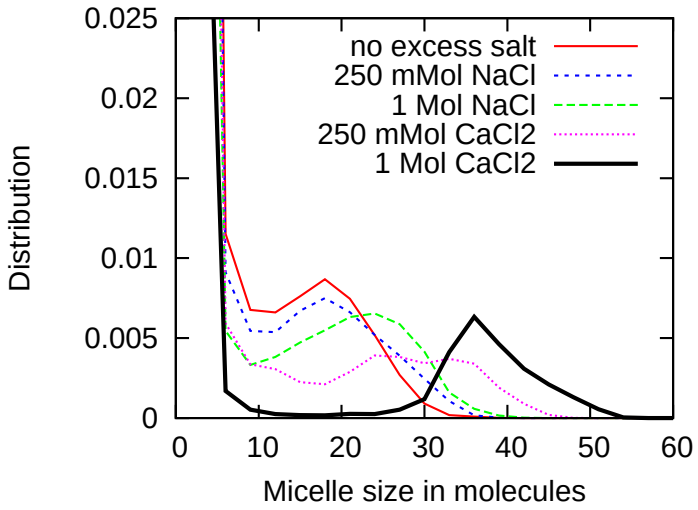

Figure 3: SHS micelle size distribution. The distribution is plotted as the average over $40-200$ ns except for the systems containing $CaCl_2$ for which the time frame is $100-200$ ns. The graphs correspond to bin size 3 and $R_{cut} = 0.4$ nm.

much larger and appear to have a more organized structure than the micelles formed either in the absence of excess salt or in the presence of monovalent NaCl. The corresponding time-averaged micelle size distributions for the 1 Mol SHS systems are presented in Fig. 3. The time averaging is performed over the part of the simulation trajectory in which a stable distribution of micelles and oligomers has formed from the random initial configuration and the distribution is no longer evolving. For systems with no excess salt, or excess monovalent NaCl, this time period is $40-200$ ns, and for the $CaCl_2$ containing systems $100-200$ ns. In line with the observations of SDS micellization in the presence of monovalent and divalent ions[33], the systems with $CaCl_2$ have slower dynamics and therefore 100 ns is considered as the initial micellization and equilibration period. Besides added salt, the micelle size distribution is sensitive to overall surfactant concentration. Micelle size distributions at 700 mMol SHS follow the 1 Mol systems but with peaks shifted toward smaller aggregates. For 700 mMol SHS systems at low ionic strength, specifically the salt-free 700 mMol SHS system, there is no separate micellization peak, although a significant number of larger aggregates are present, that is, the distribution has a tail in the aggregate sizes above 20. Both

at 1 Mol concentration and at 700 mMol SHS concentration, a small number of Ca^{2+} ions in the system shifts the micellization peak considerably toward larger aggregates.

A significant fraction of surfactants in our systems exist as monomers and oligomers. In the 700 mMol SHS system, approximately 55 % of the SHS molecules are monomers or oligomers of size 10 or smaller and the system micellizes only weakly. When NaCl is introduced at 700 mMol SHS, the number of oligomers is reduced but a clear micellization peak appears only at higher ionic strengths for 700 mMol SHS. The 1 Mol SHS system micellizes more clearly, with a much smaller number of SHS molecules as aggregates of size 10 or smaller ($5\% - 30\%$ of SHS molecules depending on the ionic strength). For the purpose of later analysis, we note that for all the systems the vast majority of non-oligomeric aggregates falls between aggregate size region $N = [10, 45]$, see Fig. 3. This size interval is used for the structural properties analysis. Thus, we cut out the oligomers and any large deformed wormlike micelles from our analysis. Notably, a small number of large aggregates in the $CaCl_2$ containing systems fall outside this region, but these correspond to deformed lumps or wormlike aggregates. Including them in the analysis would reduce the data comparability between excess sodium containing systems and calcium containing systems.

2.2 SHS micelle structure

Next, we look at SHS micelle structure. Figure 4 presents the head group and methyl group distributions in SHS micelles of sizes between $N = [10, 45]$ at 1 Mol overall concentration. We present just the data for the 1 Mol systems because the 700 mMol SHS systems are similar to the 1 Mol systems with only slight shifts towards smaller micelle radii, as the the overall micelle size distribution shifts towards smaller aggregates at lower ionic strengths. The growth in micelle size with increasing ionic strength is clearly visible in the head group distributions. However, adding NaCl has only a minor effect and the significant shift comes with the introduction of $CaCl_2$. Interestingly, the increase of micelle size upon $CaCl_2$ induces a decrease in methyl group density near the micelle center. This is due to the short chain length of the SHS molecule. For SDS this is not observed, see Refs.[31,33]. However, water and ions are still dominantly excluded from the micelle center.

Figure 5 shows the cation distribution around the SHS micelles, again for micelles

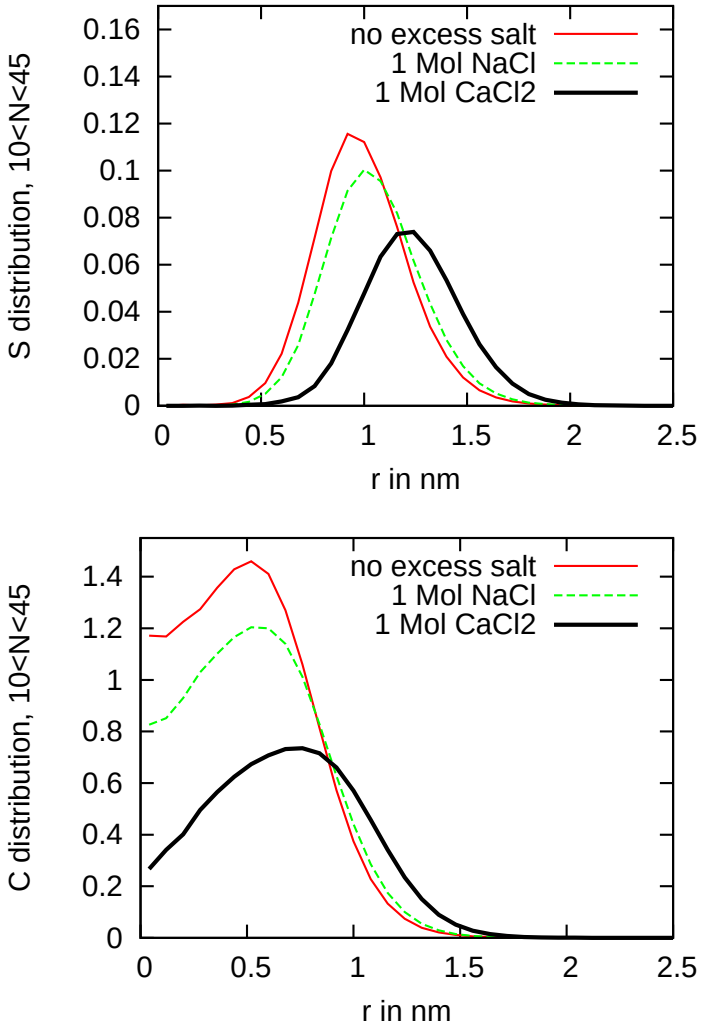

Figure 4: Head group (S) and methyl group (C) distribution in micelles of size $10 \leq N \leq 45$. The systems corresponding to the smaller concentrations of excess salt produce analogous data.

in size interval $N = [10, 45]$ at 1 Mol SHS concentration. In systems in which sodium is the only cation, i.e., systems without excess salt or systems with excess NaCl, the difference in the distributions is purely due to the number of ions in the system. However, when Ca^{2+} is present, the distributions are qualitatively different. A shift towards larger distances from the micelle center is observed due to an increase in micelle size. In addition, the Ca^{2+} effectively replaces the sodium as the counterion, that is, the monovalent sodium ions are further from the micelle center.

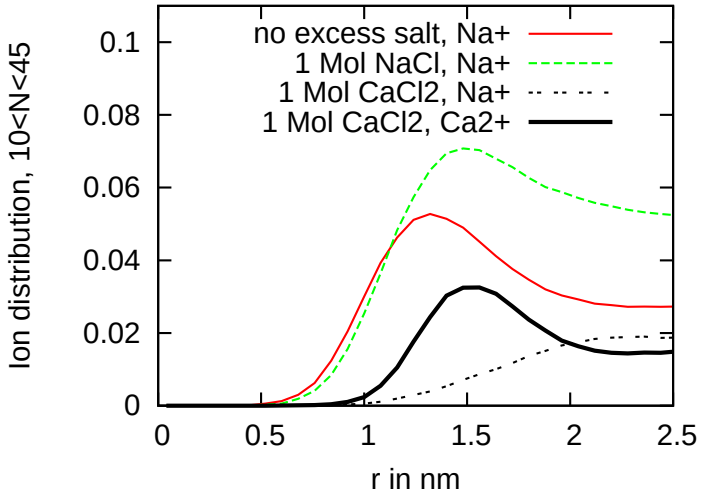

Figure 5: Cation density around micelles of size $10 \leq N \leq 45$. The introduction of $CaCl_2$ is seen as an increase in micelle size and push-out of the Na^+ ions as the counterions. The smaller concentrations of excess salt produce analogous data.

Figure 6 shows the charge distribution in and around the micelles. The head group charge shows as a dip to negative charging between 1 nm and 1.5 nm which is then countered by the cations at larger distances from the micelle center. The neutralization occurs more effectively and at a shorter distance in the presence of Ca^{2+} ions due to the shorter screening length at high ionic strength. Again, excess NaCl has very little effect in comparison to systems without excess salt. At large distances from the micelle center, the charge cumulation takes into account also the other micelles, in other words, the neighboring micelle ion coronas and headgroups.

The shift towards larger aggregates in the size distributions in Fig. 3 with an in-

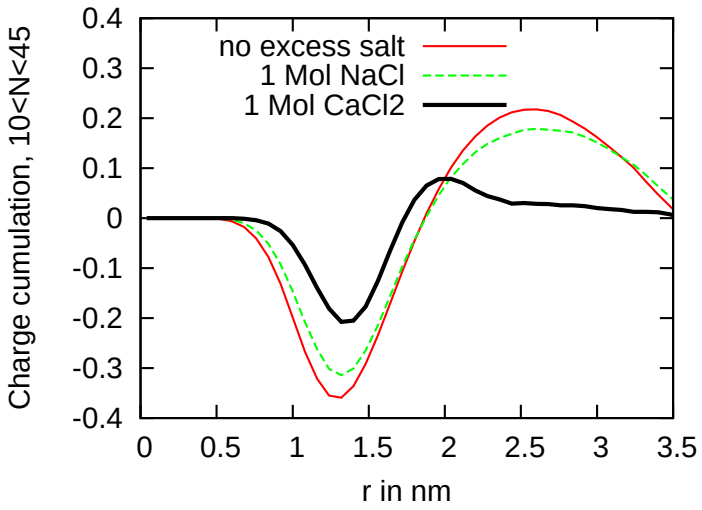

Figure 6: Cumulative charge as a function of distance from micelle center for micelles of size $10 \leq N \leq 45$. The charge is normalized by the number of SHS molecules in the micelles of size interval $[10, 45]$.

crease in ionic strength indicates an increase in micelle diameter indirectly. Additionally, the shift in head group position and methyl group distribution curves in Fig. 4, again with an increase in ionic strength, directly indicates the diameter increase. However, the question remains as to whether the aggregates are spherical, oblate, or prolate. To characterize the micelle shape, we calculated an approximation of the average radius of gyration and its principal moments for each aggregate size. The average radius of gyration is given by

$$< R_g >_x = \frac{1}{n_x} \sum_{i=1}^{n_x} \left(\lambda_{i,1}^2 + \lambda_{i,2}^2 + \lambda_{i,3}^2\right)^{1/2}, \tag{1}$$

where $\lambda_{i,1}$, $\lambda_{i,2}$, and $\lambda_{i,3}$ are the principle moments of gyration for an aggregate of size x and n_x are the number of aggregates of size x counted during the production phase of the simulation. The principle moments of gyration are the eigenvalues of the gyration tensor, S, which is defined by

$$S_{u,v} = \frac{1}{N} \sum_{i=1}^{N} \left(r_i^u - R^u\right)\left(r_i^v - R^v\right) \tag{2}$$

where r_i^u and R^u are the coordinates of particle i and the center of mass of the micelle in the u direction and N is the total number of groups in the micelle[63–65]. We found that using the actual mass of each group had a negligible effect on the radii of gyration and therefore approximated that each group had an equal mass for simplification purposes. This results in the values reported being approximations. The average radius of gyration for micelles formed in the absence of excess salt, in the presence of excess monovalent salt (NaCl), and excess divalent salt ($CaCl_2$) are presented in Fig. 7. Figure 7 shows that small aggregates have the same form regardless of the ionic strength of the solution, or the excess ion valency. However, for each ionic strength, there is a critical aggregation number at which the aggregates deviate from an approximately spherical form. This transition is relatively sharp and the point of transition shifts toward larger aggregates with increasing ionic strength. This is to be expected as the Coulombic screening length is shorter in the systems of higher ionic strength. To assess the aggregate shape further, we plotted the three main axial components of the radius of gyration in Fig. 8 for the system at highest ionic strength (1 Mol SHS with 1 Mol excess $CaCl_2$). This system was chosen as it has the widest spread of aggregate sizes and thus presents the most representative set of component spread; The systems at weaker ionic strength have an analogous behavior but with the form transition at smaller aggregate size, as seen from Fig. 7. From the component plot, we see that the aggregates formed are always slightly prolate ellipsoids. For this system at $N = 55$ SHS, the form transition seen in Fig. 7 corresponds to abrupt elongation in one axial direction, i.e., elongated spheroid form.

The lack of water penetration into the micelle center raises the question: To what degree are hydrocarbon tails exposed to water? To measure this, we evaluated the solvent accessible surface area in SDS and SHS micelles using the g_sas program[66] with solvent probe size 0.14 nm, representing a water molecule. Since SHS is weakly micellizing, there are larger numbers of monomers and oligomers present in the systems than those with more strongly micellizing surfactants. These are naturally more exposed to solvent than properly micellized molecules. For comparison purposes, we compare the solvent access of SHS molecule tails in the presence of excess $CaCl_2$, which reduces the oligomeric contribution to solvent accessible surface area value. Throughout the hydrocarbon tail, SHS has $15 - 25\%$ more solvent exposed surface than the more strongly micellizing SDS at corresponding ionic strength. This results mainly from the

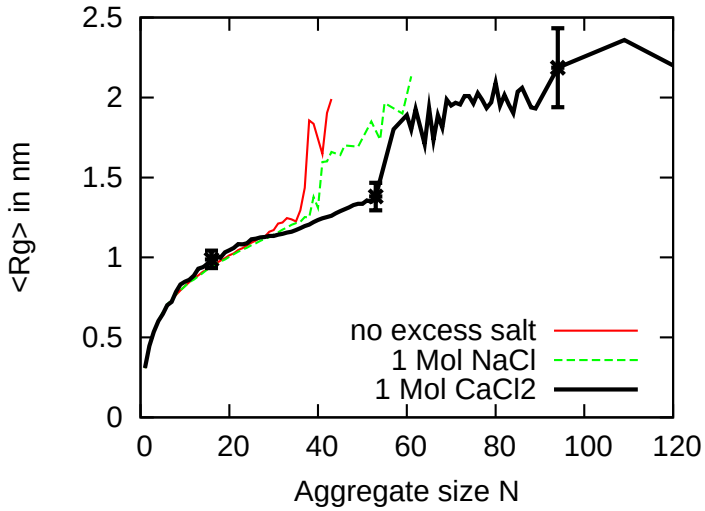

Figure 7: Average radii of gyration $< R_g >$ (see Eq. 1) based on aggregate size for 1 Mol SHS systems with and without salt. Select error bars are placed on the 1 Mol $CaCl_2$ system.

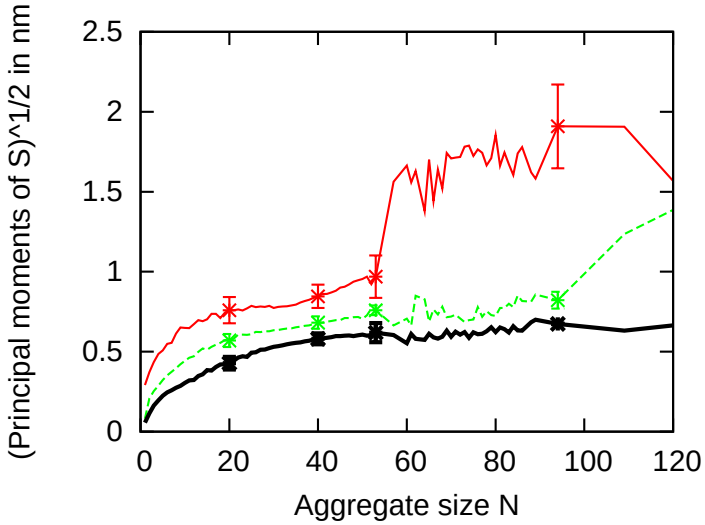

Figure 8: Square root of the principal moments of gyration S (see Eq. 2) for the aggregates of the 1 Mol SHS system with 1 Mol $CaCl_2$. Error bars are shown at select locations.

more disorganized structure of the SHS micelles.

SHS micelle structure was also characterized by the gauche defect probability. SHS has a gauche defect probability of 0.19 ± 0.01 (no excess salt/ excess NaCl) or 0.18 ± 0.01 (excess $CaCl_2$) for each bond in the hydrocarbon tail. Corresponding values for SDS are 0.16 ± 0.01 (no excess salt/ excess NaCl) or 0.14 ± 0.01 (excess $CaCl_2$) calculated from simulations data discussed in Ref.[33]. In comparison to SDS[31,33], SHS forms more disorganized micelles, as also visible in the snapshot of Fig. 1. Additionally, ionic strength sensitivity is larger in SDS micelles. For both SHS and SDS, the gauche defect probability is insensitive to concentration or addition of monovalent salt. Adding divalent salt decreases the gauche defect probability for SDS[33] but for SHS the decrease falls between the error estimate.

3 Discussion

We have investigated the critical micellization concentration, micelle size distribution, and micelle structure of an anionic surfactant, SHS, at conditions close to the experimental CMC. The simulated systems were large enough to describe consistently the micelle size distribution. Effects of increased ionic strength of solution were probed through an increase in the surfactant concentration and addition of excess sodium chloride or calcium chloride. The simulations reached equilibrium for all systems except those containing divalent salt. Our calculations match experimental measurements of critical micellization concentration and micelle size distribution[3,41,42]. Furthermore, the presence of divalent Ca^{2+} ions is observed to dominate ion condensation around the micelles, leading to more compact aggregates and slower micelle dynamics in comparison with the monovalent Na^{+}.

We initially verified that the system size of 200 SHS molecules and the duration of 200 ns is sufficient to produce a micelle size distibution that is independent of the simulation system size or initial configuration by probing various initial configurations and doubling the system size. We concluded that the system size is sufficient and we have achieved a stable distribution which we consider to represent the equilibrium distribution. We point out that the micelle dynamics in the Ca^{2+} containing systems are significantly slower than in the Na^{+} containing systems due to the formation of salt bridges, see Refs.[32,33]; For the Ca^{2+} containing systems, it is likely that the 200 ns

simulation does not encompass a representative set of dynamics events to describe true equilibrium which shows as a non-smooth micelle size distribution. Nevertheless, the Ca^{2+} containing systems also probe the equilibrium event space to a large degree.

The simulations give a critical micellization concentration of 360 ± 30 mMol or 300 ± 10 mMol for the SHS system. We did observe some variation in the calculated CMC value due to variation in the oligomer concentration between systems of different overall concentrations. The observed difference is partly due to less "free volume" for oligomers and partly to solution nonidealities. However, the calculated CMC values are close to each other and in good agreement with the experimentally reported CMC values of 420 mMol[41] and 517 mMol[42]. We also report the CMC of the model decreasing systematically with ionic strength, which is in agreement with general behavior of ionic surfactants[3,67].

At approximately 700 mMol concentration, we observe SHS to form a continuous micelle size distribution from oligomers to micelles of a maximum size of around 25 molecules. Ref.[42] reports that SHS has premicellar aggregation below the CMC. In our simulations, a significant number of SHS molecules aggregates in clusters smaller than 10 before the onset of actual micellization and the continuous aggregate size distribution we found supports this observation. At 1 Mol concentration, a proper micelle peak is observed with a maximum around aggregation number $N = 17$. Adding NaCl shifts the micelle size distribution by a few molecules towards larger aggregates. A large increase, as well as, a widening of the distribution is observed in the presence of $CaCl_2$. Experimentally, it is well-established that the aggregation number of ionic micelles grows as a function of surfactant or ion concentration[57–61]; our results agree with these observations.

SHS is a weakly micellizing surfactant. Thus very little experimental data on SHS micelle structure exist. This is also the case for longer-chain sodium alkyl sulfate micelles. We found that water and ions do not penetrate into the micellar core, but a larger number of methyl chain end groups are close to the micelle surface and exposed to water than in SDS micelles. SHS micelles are more disorganized, the hydrocarbon chains have more kinks (gauche defects), and the hydrocarbon chains in the micellar center are in a more fluidic phase than the more strongly micellizing, longer chain, sodium alkyl sulfate micelles. In Ref.[42], Suarez et al. report an organized micellar structure for SHS, but with a large exposure of alkyl chains to the solvent. Our observations fully

agree with this.

Other than the micelle size distribution peak position, the type of excess ions in the simulation system also influences micelle structure. When present, Ca^{2+} replaces Na^{+} as the condensed counterion and the resulting micelles are significantly more ordered and compact; surfactant molecules become effectively more rigid. Rigidity shows both in the dynamics and in the molecule length, or gauche defect probability. Ion interactions and their effects on longer chain sodium alkyl sulfate micelles have been studied in Refs.[29,61,68–74]. The general agreement is that the ion type and concentration affect the micelle structure and dynamics for the longer chain alkyl sulfate micelles. Reference[29] provides a comparison between Li^{+}, Na^{+}, and NH_4^{+} counterions for longer chain alkyl sulfates based on molecular dynamics simulations. Multivalent ions have been studied much less: The effects of Na^{+}, Ca^{2+}, and Al^{3+} on sodium dodecyl polyoxyethylene-2-sulfate micelles have been compared in Ref.[75] and a small concentration of multivalent ions is reported to change the micelle shape and increase the aggregation number close to CMT. This is again well in line with our observations of excess Ca^{2+} inducing much more drastic changes in micelle structure, aggregation, and dynamics than excess Na^{+}. We note that all our SHS results in saline solutions match our previous work of SDS in excess salt of Ref.[33] but represent a more disorganized system. A detailed discussion of the longer hydrocarbon chain SDS micelles in the presence of excess Na^{+} and Ca^{2+} ions is presented in Ref.[33]. It may be worth pointing out that in bilayers (and hence in liposomes), the effects of salt can also be hard to predict. It has been shown by Zhao *et al.*[76] that salt bridges may strongly promote cluster formation and the stability needed in bacterial membranes. It has also been shown that the content of a charged lipid / surfactant together with salt content is important in determining both static and dynamic properties of bilayers[77]. In micelles, the length of the hydrocarbon tail has a strong contribution to both dynamics and static properties as the difference between this study and Refs.[32,33] show.

Aggregation numbers of ionic micelles grow as a function of surfactant or ion concentration[57–61]. This is, in general, associated in small angle neutron scattering (SANS) or small angle X-ray scattering (SAXS) measurements with a structural change from spherical to elongated or worm-like micelle. Recently, Ref.[78] raised a question as to whether the structural change data could also match oblate micelles and concluded that for most of the existing experimental data an interpretation as either oblate or prolate

ellipsoids is possible. We analyzed the SHS micelle shapes at various ionic strengths and conclude that SHS forms prolate micelles at large aggregation numbers. As most of the large aggregation numbers are obtained at high ionic strengths, this is in agreement with Ref.[78] which concludes that a high ionic strength promotes prolate micelles. Furthermore, the shape analysis shows that the decrease of Coulombic screening length due to increase in ionic strength extends the aggregation number interval at which the micelles remain spherical.

To conclude, we have studied sodium hexyl sulfate micellization and equilibrium micelle structures using molecular dynamics simulations. To our knowledge, these are the first atomistic simulations of surfactant systems with explicit solvent and ions that achieve timescales required for system equilibration at concentrations comparable to experimentally reported CMCs. Given the steady advances and improvements in computational tools, we expect such atomistic simulations to yield important insights into the micellization dynamics of more complex surfactants in the near future.

Acknowledgments

This work has been supported by Academy of Finland (MS), the Natural Sciences and Engineering Research Council of Canada (MK), through NSF-DMR Grants No. 0449184 (MH) and 0819860 (Princeton Center for Complex Materials, AZP) and by the Department of Energy, Office of Basic Energy Sciences (Grant No. DE-SC-0002128, AZP). We also thank the Southern Ontario SharcNet (www.sharcnet.ca) computing facility for computer resources.

References

1. Hillmyer, M. A. *Science* **2007**, *317*(5838), 604–605.

2. Helenius, A.; Simons, K. *Biochim. Biohys. Acta* **1975**, *415*, 29–79.

3. Zana, R. *Dynamics of Surfactant Self-Assemblies: Micelles, Microemulsions, Vesicles and Lyotropic Phases*, Vol. 126; CRC Press, 2005.

4. Kékicheff, P.; Cabane, B. *J. Phys. France* **1987**, *48*, 1571–1583.

5. Kékicheff, P.; Madelmont, G. C.; Ollivon, M. *J. Coll. Interf. Sci.* **1989**, *131*, 112–132.

6. Chernik, G. G. *Curr. Opin. Colloid Interface Sci.* **1999**, *4*, 381–390.

7. Gradzielski, M. *Curr. Opin. Colloid Interface Sci.* **2004**, *9*(3-4), 256–263.

8. Peer, D.; Karp, J. M.; Hong, S.; Farokhzad, O. C.; Margalit, R.; Langer, R. *Nature Nanotechnology* **2007**, *2*, 751–760.

9. Torchilin, V. P. *Adv. Drug. Delivery Rev.* **2006**, *58*, 1532–1555.

10. Bibette, J.; Calderon, F. L.; Poulin, P. *Rep. Prog. Phys.* **1999**, *62*, 969–1033.

11. Larson, R. G. *J. Chem. Phys.* **1989**, *91*, 2479–2488.

12. Larson, R. G. *J. Chem. Phys.* **1992**, *96*, 7904–7918.

13. Dill, K. A.; Kopper, D. E.; Cantor, R. S.; Dill, J. D.; Bendedouch, D.; Chen, S. H. *Nature* **1984**, *309*, 42–46.

14. Dill, K. A.; Flory, P. J. *Proc. Natl. Acad. Sci* **1981**, *78*, 676–680.

15. Dill, K. A. *J. Phys. Chem.* **1982**, *86*, 1498–1500.

16. Goetz, R.; Lipowsky, R. *J. Chem. Phys.* **1998**, *108*, 7397–7409.

17. Bandyopadhyay, S.; Klein, M. L.; Martyna, G. J.; Tarek, M. *Mol. Phys.* **1998**, *95*, 377–384.

18. Gao, J.; Ge, W.; Hu, G.; Li, J. *Langmuir* **2005**, *21*, 5223–5229.

19. Cheong, D. W.; Panagiotopoulos, A. Z. *Langmuir* **2006**, *22*, 4076–4083.

20. Jusufi, A.; Hynninen, A.-P.; Panagiotopoulos, A. Z. *The Journal of Physical Chemistry B* **2008**, *112*(44), 13783–13792.

21. Jusufi, A.; Hynninen, A.-P.; Haataja, M.; Panagiotopoulos, A. Z. *The Journal of Physical Chemistry B* **2009**, *113*(18), 6314–6320.

22. Sanders, S. A.; Panagiotopoulos, A. Z. *The Journal of Chemical Physics* **2010**, *132*(11), 114902+.

23. Drouffe, J. M.; Maggs, A. C.; Leibler, S. *Science* **1991**, *254*, 1353–1356.

24. Mackerell, A. D. *J. Phys. Chem.* **1995**, *99*, 1846–1855.

25. Tieleman, D. P.; van der Spoel, D.; Berendsen, H. J. C. *J. Phys. Chem. B* **2000**, *104*.

26. Marrink, S. J.; Tieleman, D. P.; Mark, A. E. *J. Phys. Chem. B* **2000**, *104*, 12165–12173.

27. Bruce, C. D.; Senapati, S.; Berkowitz, M. L.; Perera, L.; Forbes, M. D. E. *J. Phys. Chem. B* **2002**, *106*, 10902–10907.

28. Yamamoto, S.; Maruyama, Y.; Hyodo, S. A. *J. Chem. Phys.* **2002**, *116*(13), 5842–5849.

29. Rakitin, A. R.; Pack, G. R. *J. Phys. Chem. B* **2004**, *108*, 2712–2716.

30. Yakolev, D.; Boek, E. *Langmuir* **2007**, *23*, 6588–6597.

31. Sammalkorpi, M.; Karttunen, M.; Haataja, M. *J. Phys. Chem. B* **2007**, *111*(40), 11722–11733.

32. Sammalkorpi, M.; Karttunen, M.; Haataja, M. *J. Am. Chem. Soc.* **2008**, *130*(0), 17977–17980.

33. Sammalkorpi, M.; Karttunen, M.; Haataja, M. *The Journal of Physical Chemistry B* **2009**, *113*(17), 5863–5870.

34. Lazaridis, T.; Mallik, B.; Chen, Y. *J. Phys. Chem. B* **2005**, *109*, 15098–15106.

35. Esposito, C.; Colicchio, P.; Facchiano, A.; Ragone, R. *J. Colloid Interface Sci.* **1998**, *200*, 310–312.

36. Gu, G.; Yan, H.; Chen, W.; Wang, W. *J. Coll. Interf. Sci.* **1996**, *178*, 614–619.

37. Johnson, I.; Olofsson, G.; Jönsson, B. *J. Chem. Soc. Faraday Trans. 1* **1987**, *83*.

38. Joshi, T.; Mata, J.; Bahadur, P. *Colloids Surf., A* **2005**, *260*, 209–215.

39. Cifuentes, A.; Bernal, J.; Masa, D. J. C. *Anal. Chem.* **1997**, *69*, 4271–4274.

40. Bastiat, G.; Grassl, B.; Khoukh, A.; Francois, J. *Langmuir* **2004**, *20*, 5759–5769.

41. Rassing, J.; Sams, P. J.; Wyn-Jones, E. *J. Chem. Soc., Faraday Trans. 2:* **1974**, *70*, 1247–1258.

42. Suarez, M. J.; Lopez-Fontan, J. L.; Sarmiento, F.; Mosquera, V. *Langmuir* **1999**, *15*(16), 5265–5270.

43. Berendsen, H. J. C.; van der Spoel, D.; van Drunen, R. *Comp. Phys. Comm.* **1995**, *91*, 43–56.

44. Lindahl, E.; Hess, B.; van der Spoel, D. *J. Mol. Mod.* **2001**, *7*(8), 306–317.

45. van der Spoel, D.; Lindahl, E.; Hess, B.; Groenhof, G.; Mark, A. E.; Berendsen, H. J. *J. Comput. Chem.* **2005**, *26*(16), 1701–1718.

46. Berendsen, H. J. C.; Postma, J. P. M.; van Gunsteren, W. F.; Dinola, A.; Haak, J. R. *J. Chem. Phys.* **1984**, *81*, 3684–3690.

47. Hess, B.; Bekker, H.; Berendsen, H. J. C.; Fraaije, J. G. E. M. *J. Comp. Chem.* **1997**, *18*, 1463–1472.

48. Miyamoto, S.; Kollman, P. A. *J. Comput. Chem.* **1992**, *13*(8), 952–962.

49. Essman, U.; Perela, L.; Berkowitz, M. L.; Darden, T.; Lee, H.; Pedersen, L. G. *J. Chem. Phys.* **1995**, *103*, 8577–8592.

50. York, D. M.; Darden, T. A.; Pedersen, L. G. *J. Chem. Phys.* **1993**, *99*, 8345–8348.

51. Patra, M.; Karttunen, M.; Hyvönen, M. T.; Falck, E.; Vattulainen, I. *J. Phys. Chem. B* **2004**, *108*, 4485–4494.

52. Patra, M.; Hyvönen, M. T.; Falck, E.; Sabouri-Ghomi, M.; Vattulainen, I.; Karttunen, M. *Comput. Phys. Comm.* **2007**, *176*(1), 14–22.

53. Patra, M.; Karttunen, M. *J. Comput. Chem.* **2004**, *25*(5), 678–689.

54. Auffinger, P.; Cheatham, T. E.; Vaiana, A. C. *J. Chem. Theory Comput.* **2007**, *3*(5), 1851–1859.

55. Berendsen, H. J. C.; Postma, J. P. M.; van Gunsteren, W. F.; Hermans, J. In *Intermolecular Forces*; Pullman, B., Ed.; Reidel: Dordrecht, 1981; pages 331–342.

56. Humphrey, W.; Dalke, A.; Schulten, K. *J. Molec. Graphics* **1996**, *14*, 33–38.

57. Hall, D. G. *Langmuir* **1999**, *15*, 3483–3485.

58. Croonen, Y.; Geladé, E.; van der Zegel, M.; van der Auweraer, M.; Vandendriessche, H.; de Scgryver, F. C.; Almgren, M. *J. Phys. Chem* **1983**, *87*, 1426–1431.

59. Quina, F. H.; Nassar, P. M.; Bonilha, P. M.; Bales, B. L. *J. Phys. Chem.* **1995**, *99*, 17028–17031.

60. Bales, B. L.; Messina, L.; Vidal, A.; Peric, M.; Nascimiento, O. R. *J. Phys. Chem. B* **1998**, *102*, 10347–10358.

61. Griffiths, P. C.; Paul, A.; Heenan, R. K.; Penfold, J.; Ranganathan, R.; Bales, B. L. *J. Phys. Chem. B* **2004**, *108*, 3810–3816.

62. Floriano, M. A.; Caponetti, E.; Panagiotopoulos, A. Z. *Langmuir* **1999**, *15*(9), 3143–3151.

63. Theodorou, D. N.; Suter, U. W. *Macromolecules* **1985**, *18*(6), 1206–1214.

64. Janszen, H. W. H. M.; Tervoort, T. A.; Cifra, P. *Macromolecules* **1996**, *29*(17), 5678–5687.

65. Cheng, L.; Cao, D. *Langmuir* **2009**, *25*(5), 2749–2756.

66. Eisenhaber, F.; Lijnzaad, P.; Argos, P.; Sander, C.; Scharf, M. *Journal of Computational Chemistry* **1995**, *16*(3), 273–284.

67. Corrin, M. L.; Harkins, W. D. *Journal of the American Chemical Society* **1947**, *69*(3), 683–688.

68. Mazer, N. A.; Benedek, G. B.; Carey, M. C. *J. Phys. Chem.* **1976**, *80*, 1075–1085.

69. Lebedeva, N. V.; Shahine, A.; Bales, B. L. *J. Phys. Chem. B* **2005**, *109*, 19806–19816.

70. Hayashi, S.; Ikeda, S. *J. Phys. Chem.* **1980**, *84*, 744–751.

71. Srinivasan, V.; Blankschtein, D. *Langmuir* **2003**, *19*, 9932–9945.

72. Tcacenco, C. M.; Zana, R.; Bales, B. L. *J. Phys. Chem. B* **2005**, *109*, 15997–16004.

73. Aswal, V. K.; Goyal, P. S. *Phys. Rev. E* **2003**, *67*.

74. Vasilescu, M.; Angelescu, D.; Caldararu, H.; Almgren, M.; Khan, A. *Colloids Surf., A* **2004**, *235*(1-3), 57–64.

75. Alargova, R.; Petkov, J.; Petsev, D.; Ivanov, I. B.; Broze, G.; Mehreteab, A. *Langmuir* **1995**, *11*, 1530–1536.

76. Zhao, W.; Rog, T.; Gurtovenko, A.; Vattulainen, I.; Karttunen, M. *Biophysical Journal* **2007**, *92*(4), 1114–1124.

77. Miettinen, M. S.; Gurtovenko, A. A.; Vattulainen, I.; Karttunen, M. *The Journal of Physical Chemistry B* **2009**, *113*(27), 9226–9234.

78. Vass, S.; Pedersen, J. S.; Plestil, J.; Laggner, P.; Retfalvi, E.; Varga, I.; Gilanyi, T. *Langmuir* **2008**, *24*(2), 408–417.